Use of a simple model for studying oceanic tracer distributions and the global carbon cycle

By U. SIEGENTHALER and F. JOOS, *Physics Institute, University of Bern, CH-3012 Bern, Sidlerstrasse 5, Switzerland*

ABSTRACT

We have studied, based on work of Shaffer and Sarmiento (1992), a model for simulating the transport of CO_2 and tracers in the ocean (HILDA, for High-Latitude Exchange/Interior Diffusion-Advection Model) that combines features of box models and of the box-diffusion model. It is latitudinally divided into two zones; in the low latitudes, transport into the deep ocean occurs by eddy diffusion, while the high-latitude zone consists of two boxes (surface and deep ocean). We compare different ways of calibration and find that in order to reproduce the distributions of natural ^{14}C as well as of bomb-produced ^{14}C, the vertical eddy diffusivity K must decrease with depth. The concept of eddy diffusion is discussed by calculating apparent eddy diffusivities from 3-D model tracer simulations. The depth dependence of K is qualitatively confirmed by these calculations, reflecting the fact that the water circulation is more vigorous near the surface than at depth. We find that eddy diffusivities derived from ^{14}C are not appropriate for representing the large-scale vertical temperature distribution, because the latitudinal distribution of temperature differs in a systematic way from that of ^{14}C and also of anthropogenic CO_2. Oceanic uptake of anthropogenic CO_2, biospheric CO_2 emissions and isotopic perturbations are calculated, based on the observed atmospheric CO_2 concentration history. The results indicate an oceanic uptake of 1.9 Gt C yr^{-1} in 1980 and a near-zero net contribution from the biota in the past several decades. The HILDA model is compared with other models, and we find that its response to atmospheric CO_2 perturbations is rather similar to that of a 3-D ocean carbon cycle model of Sarmiento et al. (1992).

1. Introduction

Many global-scale studies of oceanic tracer transport or of the cycle of carbon and other elements have been performed using box-type models which have a very coarse spatial resolution and in which ocean dynamics is not calculated, but prescribed in a parameterized way. These simplified models cannot be used for simulating oceanic transport with realistic topography and boundary conditions. Three-dimensional General Ocean Circulation Models have been developed for this purpose which compute ocean dynamics based on physical principles.

General Ocean Circulation Models are being used for studying problems related to global change, but they are expensive regarding computer resources and programming time, which restricts the number of possible studies. Furthermore, the interpretation of the results of three-dimensional models is not always easy in view of the numerous processes and feedbacks they comprise. Therefore, simplified schemes, like box models or diffusion-advection models, continue to be important tools for understanding the global ocean. In particular, they provide a valuable framework for studying the influence of specific processes or imposed changes. The art of building simple models consists in finding which features and processes are of primary importance for the question under consideration and in determining the appropriate values of the model parameters, making use of analogies e.g. between excess CO_2 invading the ocean and transient tracers like bomb-produced ^{14}C. If properly devised and calibrated, a simple model can provide an economic quantitative tool, for instance for estimating how much excess CO_2 is taken up by the ocean. Thus, the oceanic CO_2

uptake has so far often been estimated using box-type models.

A typical simple model is the box-diffusion model, originally developed by Oeschger et al. (1975) for studying the cycle of carbon between ocean and atmosphere and in particular the fate of anthropogenic CO_2, and later often used also by other authors. The box-diffusion model is purely 1-dimensional; it therefore neglects the variation of vertical transport rates with latitude which may be quite important, as the vertical exchange between surface and deep ocean layers is particularly rapid in high latitudes, where the stratification is weak. In order to estimate the effect of this, Siegenthaler (1983) expanded the box-diffusion model by adding direct ventilation of the deep waters via an outcrop area in high latitudes. This outcrop-diffusion ocean indeed takes up significantly more CO_2 than the box-diffusion model without outcrop. However, it is based on the extreme assumption that the transport from the outcrop at the surface to depth is infinitely fast. In this way, the uptake of CO_2 must be over-estimated. Another simple model is a three-box ocean model, consisting of two surface reservoirs each in exchange with the atmosphere and with a deep-sea box, which was used by Knox and McElroy (1984), Sarmiento and Toggweiler (1984) and Siegenthaler and Wenk (1984) for studying the importance of high-latitude oceanic processes for natural CO_2 variations.

Here, we use a scheme that builds on these models and retains their simplicity, but in which the high-latitude transports are integrated in a somewhat more realistic way. This High-Latitude Exchange/Interior Diffusion-Advection (HILDA) model, devised by Shaffer and Sarmiento (1992) for simulating the oceanic distribution of natural properties, essentially consists of an advective-diffusive ocean at low latitudes to which two high-latitude boxes (surface and deep) are coupled. While Shaffer and Sarmiento concentrated on steady-state distributions of oceanic properties using analytical solutions, we also consider transient signals like anthropogenic CO_2, bomb-produced ^{14}C and chlorofluorocarbons. For this purpose we have developed a numerical version of the model. We discuss in this paper in detail the calibration of the model, in particular the question whether it is possible to simultaneously reproduce the distributions of several steady-state and transient properties, such as natural ^{14}C,

bomb-produced ^{14}C and temperature, which are governed by different transport processes and time scales. Apparent eddy diffusivities are calculated from 3-D model simulations. We then use the model to study the anthropogenic perturbations of the concentration as well as the isotopic composition of atmospheric CO_2 and compare with the results from other models.

2. Model description

The High-Latitude Exchange/Interior Diffusion-Advection (HILDA) model includes two well-mixed surface boxes, in low (LS) and in high latitudes (HS), a well-mixed high-latitude deep water box (HD), an advective-diffusive Interior deep water reservoir and a well-mixed atmosphere (see Fig. 1). (Our structure differs slightly from that adopted by Shaffer and Sarmiento (1992) in
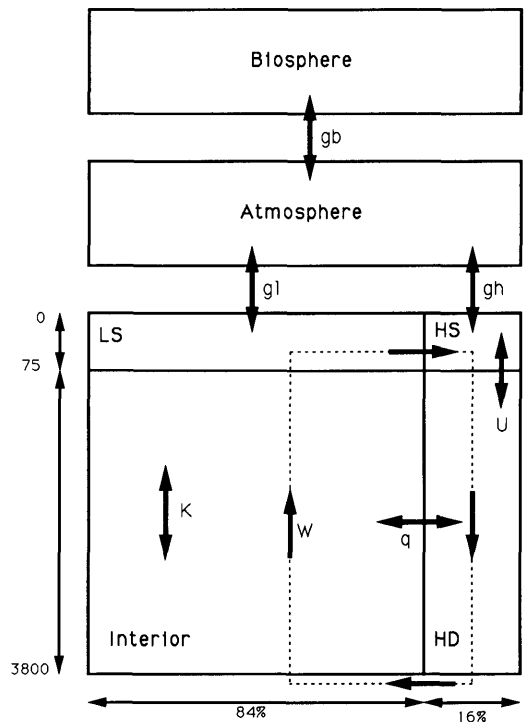

Fig. 1. Structure of the HILDA model. The biosphere box is included only for calculating isotopic perturbations due to the anthropogenic CO_2 emissions, i.e., the Suess effect.

that they did not include surface reservoirs of finite size.) The high-latitude box HS includes the regions with an annual mean surface temperature of less than 5°C, corresponding to the Antarctic Ocean south of approximately 52°S and parts of the northern North Atlantic; it covers 16% of the global ocean surface. Water transport is described by 4 parameters: an eddy diffusivity K, an advective flux w (upwelling in the interior box and downwelling in the high latitudes), an exchange flux u between HS and HD, and an exchange flux q between HD and interior box, assumed independent of depth. A constant pCO_2 of 280 ppm is assumed in all surface waters. A constant concentration of dissolved inorganic carbon (ΣCO_2) of 2.053 mol m^{-3}, representative for surface waters in low and mid-latitudes, is adopted for the whole pre-industrial ocean. In reality, deep waters have 10 to 20% higher ΣCO_2 concentration and the total carbon content of the ocean is larger than in our model, but for the applications considered here, this is of little importance. The surface

boxes exchange CO_2 with the atmosphere. The gas exchange coefficient (flux of CO_2 per unit concentration difference air-sea) is assumed equal in low and in high latitudes. This is actually not the case, since the gas exchange depends on wind speed and winds are significantly stronger in high than in lower latitudes. We follow, however, the argument of Shaffer and Sarmiento that sea ice partly suppresses gas exchange in winter, which roughly compensates the influence of high wind speeds, so that the annual mean gas exchange in the oceanic regions represented by the HS box may be about equal to that in lower latitudes. The values of the model quantities and parameters are given in Table 1.

For carrying out time-dependent simulations, we set up a numerical model version, in which the Interior ocean reservoir is vertically split into 68 boxes, 25 m thick from 75 m depth (bottom of the LS box) to 1100 m depth and 100 m thick below 1100 m. Time integration is performed using a 4th order Runge-Kutta scheme with variable

Table 1. *Values of fixed and adjustable model parameters*

Fixed quantities			
CO_2 concentration in pre-industrial atmosphere		280 ppm	
CO_2 mass in pre-industrial atmosphere		594.4 Gt C	
Carbon concentration in pre-industrial ocean		2.053 mol m^{-3}	
Ocean surface area, A_s		$3.62 \cdot 10^{14}$ m^2	
Mean residence time of carbon in biosphere		20 yr	
$^{13}C/^{12}C$ fractionation factors:			
atmosphere → LS box		$1 - 1.78\,°/_{oo}$	
LS box → atmosphere		$1 - 9.98\,°/_{oo}$	
atmosphere → HS box		$1 - 1.87\,°/_{oo}$	
HS box → atmosphere		$1 - 12.37\,°/_{oo}$	
atmosphere → biosphere		$1 - 18.13\,°/_{oo}$	
biosphere → atmosphere		$1 - 0\,°/_{oo}$	
Adjustable parameters			
Model version	STST	BOMB	$K(z)$
eddy diffusivity K (m^2 yr^{-1})	853	4700	see text
gas exchange rate at 280 ppm (mol m^{-2} yr^{-1}), $g_1 = g_h$	15.1	15.2	15.1 ± 1.2
high-latitude exchange (HS − HD), u (m yr^{-1})	53	53	38 ± 17
upwelling velocity in interior box, w (m yr^{-1})	0.70	0.70	0.44 ± 0.56
(exchange coeff.)$^{-1}$ Interior-HD box relative to interior volume, q^{-1} (yr)	420	420	538 ± 510

See also Fig. 1. The errors on the parameters were obtained using a covariance technique, based on uncertainties of the data used for calibration. $^{13}C/^{12}C$ fractionation factors were calculated after Siegenthaler and Münnich (1981) and Mook (1986).

time step. For some steady state properties (temperature and pre-industrial ^{14}C), an analytical solution of the model equations can be found (Shaffer and Sarmiento, 1992), as long as all transport parameters are independent of depth (i.e., for versions STST and BOMB, see below). For these properties, the numerically obtained distributions agree very well with the analytical solution.

3. Model calibration: determination of the transport parameters

For models like HILDA, an essential problem is to determine appropriate numerical values for the transport parameters. The way to do this is to use observations of oceanic tracers that behave analogously as the property to be studied (for instance anthropogenic CO_2) and to determine the model parameters such as to reproduce those observations. We have performed three different calibrations: First, using the steady-state distributions of temperature and pre-bomb ^{14}C (version STST); second, using the distribution of bomb-produced ^{14}C (version BOMB). These two versions both have a depth-independent eddy diffusivity K. The numerical values of the transport parameters, particularly of K, obtained for versions STST and BOMB differ considerably (see below); the same thing was found earlier for the box-diffusion model (Siegenthaler, 1983). In order to overcome the unsatisfactory situation that the model cannot reproduce the distributions of natural ^{14}C and of bomb-^{14}C with the same set of parameters, we abandoned the restriction that the eddy diffusivity should be constant with depth. This led to the third calibration, using the distribution of natural as well as of bomb-produced ^{14}C (version $K(z)$). Temperature was not used for this last calibration, as discussed below.

The transport parameters K, u, w and q were determined by an iterative least squares method, minimizing the weighted sum of squares of the differences between model-calculated and prescribed values.

The *data basis* used is as follows. Temperature values were adopted from the paper by Shaffer and Sarmiento (1992), who calculated mean values based on the compilation by Levitus (1982), for the well-mixed boxes LS, HS and HD, and for

equidistant depth levels 500 m apart in the Interior reservoir. ^{14}C concentrations are indicated here in the $\Delta^{14}C$ notation, giving the deviation (in permil) of the ^{13}C-normalized concentration from a standard value (Stuiver and Pollach, 1977). In this notation, the pre-industrial value for the atmosphere was near 0 permil. Oceanic mean ^{14}C concentrations, calculated from values from the GEOSECS data, were obtained from Shaffer and Sarmiento (1992) and from G. Shaffer (personal communication). The GEOSECS observations actually cover the period 1972–1978 for the different ocean basins; we chose as a representative date 1 January 1974, since the Pacific Ocean Expedition took part in 1973/74 and the Pacific is the largest ocean. The $\Delta^{14}C$ value for the LS box at this date was chosen as 110 permil (Tans, 1981). The pre-industrial $\Delta^{14}C$ values adopted for the LS and HS boxes are -40 and -120 permil. Pre-industrial $\Delta^{14}C$ at $\geqslant 1000$ m depth is taken from the GEOSECS data, since bomb-^{14}C had in general not penetrated so deep down. We calculated the total oceanic inventory of bomb-^{14}C

Table 2. *Prescribed data used for calibrating the model, and values calculated with the model; the uncertainties indicated for the prescribed values are those assumed in the error analysis of the transport parameters for version $K(z)$*

| | Steady-state $\Delta^{14}C$ ($^{o}/_{oo}$) | | $\Delta^{14}C$ 1-1-1974 ($^{o}/_{oo}$) | |
	Prescribed	HILDA $K(z)$	Prescribed	HILDA $K(z)$
HS box	-120 ± 30	-111	-5 ± 30	-10
HD box	—	-136	-125 ± 30	-123
LS box	-40 ± 20	-45	110 ± 20	112.6
Interior:				
300 m	—	-57	4 ± 20	19
500 m	-87 ± 20	-74	—	-53
600 m	—	-85	-80 ± 20	-81
1000 m	-141 ± 10	-133	—	-133
1500 m	-172 ± 10	-170	—	-170
2000 m	-184 ± 10	-182	—	-182
2500 m	$-187-10$	-185	—	-185
3000 m	-187 ± 10	-183	—	-183
3500 m	-184 ± 10	-176	—	-176
Inventory of bomb-^{14}C, 1-1-1974 (10^{-10} mol ^{14}C m^{-2})			1.33 ± 0.20	1.32
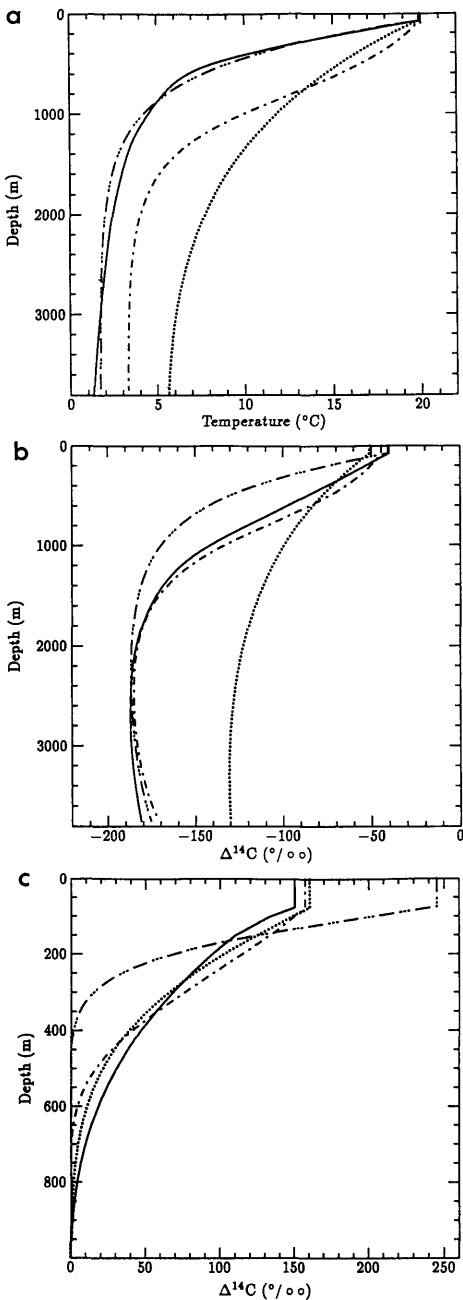
Fig. 2. Model-simulated as well as observed (or prescribed) oceanic distributions of (a) temperature, (b) steady-state ^{14}C and (c) bomb-produced ^{14}C (see also Table 2). Line signatures: Solid: prescribed distribution (smooth line through the actual data points); model-calculated distributions: · · · — · · · — version STST, · · · · · version BOMB, · — · — version $K(z)$.

from the regional inventories assessed by Broecker et al. (1985). Prescribed values for ^{14}C are given in Table 2 and shown in Fig. 2.

(1) *Steady state calibration (STST)*. This calibration was carried out essentially in the same way as by Shaffer and Sarmiento (1992), using temperatures and pre-industrial ^{14}C concentrations. Since the numerical values of the two quantities are not directly comparable, they must be scaled by weight factors in the least squares calibration procedure. We used the same weight as Shaffer and Sarmiento, namely $1/(x_{min} - x_{max})^2$, where the bracket gives a representative range spanned by each quantity (20°C and 180 permil, respectively). The gas exchange coefficient was determined such that the net flux into the ocean, assuming an atmospheric Δ^{14}C value of 0 permil, matches the radioactive decay of ^{14}C in the ocean. The resulting transport parameter values are given in Table 1.

(2) *Calibration using bomb-produced ^{14}C (version BOMB)*. Using the parameters of version STST, the distribution of bomb-produced ^{14}C is not well reproduced, with too high a surface concentration and too low a column-integrated inventory in low-latitude waters, i.e., the vertical mixing in the top several 100 m of the Interior reservoir is too sluggish. We therefore carried out another calibration, using as target values the observed surface water ^{14}C concentration for the LS box and the global inventory of bomb-^{14}C, both at the time of GEOSECS. From these two conditions we determined the eddy diffusivity and the gas exchange flux; the values adopted for u, q and w are those from version STST. The calibration runs were carried out prescribing the atmospheric CO_2 concentration as a function of time, as given by direct monitoring and by ice core data (see Section 6 below). The atmospheric ^{14}C concentration change until 1954, due to dilution with ^{14}C-free fossil-fuel CO_2, was calculated; from then on (influence of nuclear weapon tests), atmospheric ^{14}C was prescribed according to observations (Tans, 1981). The eddy diffusivity, K, obtained from the bomb-^{14}C calibration is 4700 m^2 yr^{-1}, much larger than the value obtained from the calibration using the steady state tracers (853 m^2 yr^{-1}).

While version BOMB correctly reproduces the net uptake of bomb-^{14}C, it yields too high values for the natural ^{14}C concentration in the deep ocean (Fig. 2b). Obviously, it is not possible to

simultaneously reproduce the oceanic inventories of natural and of bomb-produced ^{14}C with one set of parameters. This indicates that neither of the first two model versions can give reliable estimates of surface-to-depth tracer transport on significantly different time scales; version STST is appropriate for characteristic times $\tau \approx 10^3$ years and version BOMB for $\tau \approx 10$ years. This is an unsatisfactory situation; it can be changed by dropping the restriction that the eddy diffusivity K is constant with depth, as we did for the third model version.

(3) *Depth-dependent eddy diffusivity K, version $K(z)$.* We assumed for this version that K decreases with depth, which leads to relatively fast downward transport of bomb-^{14}C in the surface-near layers of the Interior reservoir and to slow transport in the bulk of the deep ocean where the major part of the natural ^{14}C is situated. We assumed a K profile of the form (z: depth below surface; $z_{LS} = 75$ m depth of the LS box)

$$K(z) = K_0 + K_1 \exp(-[z - z_{LS}]/z_0). \qquad (1)$$

Target values for this version were pre-industrial ^{14}C concentrations as in STST but with an additional value at 500 m depth (obtained by linear interpolation between 75 and 1000 m depth), ^{14}C concentrations in 1974 at the depth levels shown in Table 2, and, with a large weight, the global inventory of bomb-produced ^{14}C. Temperatures were not prescribed as target values, because we found that it is not possible to satisfactorily reproduce the distributions of temperature and ^{14}C simultaneously with this model (see next section). The resulting values for the $K(z)$ profile are $K_0 = 465$ m^2 yr^{-1}, $K_1 = 7096$ m^2 yr^{-1} and $z_0 = 253$ m. Thus, K decreases rapidly with depth: $K = 7561$ m^2 yr^{-1} at the bottom of the mixed layer $(z = z_{LS})$, $K(500$ m$) = 1788$ m^2 yr^{-1} and $K(1000$ m$) = 648$ m^2 yr^{-1}.

In version, $K(z)$, the exchange rate u between the two high-latitude boxes, HS and HD, as determined by the ^{14}C distributions, is lower (38 m yr^{-1}) than found in version STST (53 m yr^{-1}) where it is essentially determined by temperature. The u value of the $K(z)$ version is preferable, since it has been obtained using a time-dependent tracer.

The gas exchange fluxes at 280 ppm obtained in the different versions agree well: 15.1 mol m^{-2} yr^{-1}

in versions STST and $K(z)$, 15.2 mol m^{-2} yr^{-1} in version BOMB. This flux is at the lower end of the range obtained by other authors (Broecker et al., 1980; Stuiver et al., 1981; Siegenthaler, 1986). One reason is that we assumed a constant concentration of ΣCO_2 for the whole ocean, equal to the surface value, which is about 12% less than the actual mean oceanic value. Furthermore, the bomb-^{14}C inventory of Broecker et al. (1985), which we use here, is about 10% lower than that used by the earlier authors who had a less complete data set at their disposition. Our flux is also lower than the value of about 17.5 mol m^{-2} yr^{-1} at 280 ppm obtained by Broecker et al. (1985), although we used their data for calculating the bomb-^{14}C inventory. Reasons for our smaller value may be regional inhomogeneities of the inventories and concentrations that were taken into account by Broecker et al., but not by us, and somewhat different ^{14}C time histories assumed for calculating the flux of bomb-^{14}C into the ocean. Further, we considered in our calculation the anthropogenic CO_2 increase which leads to an additional transport of ^{14}C via the net flux of CO_2 into the ocean, which was not taken into account by Broecker et al.

Table 1 also gives errors on the transport parameters, determined using covariance analysis (Junkins, 1978), for version $K(z)$ corresponding to the uncertainties of the data used for calibration as given in Table 2. The error of the eddy diffusivity $K(z)$ depends on the depth; it is between 30 and 50% in the top 500 m of the Interior reservoir. An isolated discussion of the magnitude of the errors of the parameter is not very meaningful; their effect will be seen below when we determine the uncertainty of quantities like the airborne fraction.

4. Distributions of temperature and ^{14}C, limits of box models

Figs. 2a–c show the model-simulated as well as the observed (or prescribed) depth distributions of temperature, steady-state ^{14}C and bomb-produced ^{14}C (see also Table 2). Except for the STST version, which was calibrated using temperature, the Interior is too warm in the model. Pre-industrial ^{14}C concentrations are reasonably well simulated by version $K(z)$, too low above 1500 m depth in

version STST and too high below 500 m in version BOMB. The distribution of bomb-produced ^{14}C in the Interior reservoir is well represented by version BOMB and also by $K(z)$, while version STST yields too high surface values and too small an oceanic inventory (by 12%), in other words too small a penetration depth. In version $K(z)$, the penetration depth of bomb-^{14}C is slightly smaller than prescribed, but we do not consider this as a serious deviation, since the detailed depth distribution of ^{14}C in pre-bomb time, and consequently also that of the net bomb signal, is not very well known.

What are the causes for the differences between the three versions? For answering this, let us first consider under what conditions a box model is an appropriate representation of reality. Representing some region of the ocean by a "well-mixed" box is obviously in order if the region is internally mixed in a short time compared to the time scales of the fluxes, but this is only a special case. The box representation is generally justified if each water

Fig. 3. Zonal-average surface values of temperature (thick solid line), pre-industrial ^{14}C, net bomb-produced ^{14}C (GEOSECS observations minus pre-bomb distribution) and anthropogenic CO_2 (expressed as partial pressure, pCO_2; thin solid line) versus latitude. The results are plotted using a normalized scale from -1 ($=$ a representative deep-sea value; $2°C$, $-160\,°/_{oo}$, $0\,°/_{oo}$ and 0 ppm, respectively) to 0 ($=$ average value in the region $52°S$ to $63°N$, corresponding to the LS box; $19.9°C$, $-60\,°/_{oo}$, $178\,°/_{oo}$ and, 59.1 ppm, respectively). Values are zonal means for the world ocean for temperature (data from Levitus, 1982) and pCO_2 (Sarmiento et al., 1992), and for the Atlantic plus Pacific Oceans for ^{14}C (data from Broecker and Peng, 1982). Vertical lines denote the latitude of $5°C$ sea surface temperature and thus the approximate LS $-$ HS boundary in HILDA.

parcel in the region has an equal probability to be affected by the considered fluxes (i.e., transport paths, sources and sinks). A box representation is, however, in many situations also appropriate under weaker conditions. An important case is the simulation of tracers which have a relatively homogeneous concentration in the considered region. In Fig. 3, zonally averaged sea-surface values of temperature, pre-industrial ^{14}C and bomb-produced ^{14}C are plotted versus latitude, using a scale from -1 (corresponding to a representative deep-sea value) to 0 (average value in the region $52°S$ to $63°N$, represented by the LS box). In the LS region, the ^{14}C concentrations of all water parcels are in a restricted range, and all water parcels mixed down from the low- and mid-latitude surface carry, in a good approximation, the horizontally averaged surface ^{14}C concentration. An analogous argument holds for the ^{14}C content of the CO_2 evading from the LS box into the atmosphere. Therefore, lumping all surface water warmer than $5°C$ into one box seems to be a reasonable approach for ^{14}C.

Turning to temperature, we first note that the model temperature value at some location also indicates the relative contribution of water originating from the high-latitude and the low-latitude surface, because every water parcel is a mixture of these two end-members in the model. For a water parcel with temperature T, the fraction f_{HS} of the component originating from HS is given by

$$f_{HS} = \frac{T - T_{LS}}{T_{HS} - T_{LS}}, \qquad (2)$$

where T_{LS} and T_{HS} are the temperatures in the respective boxes. At the same time, the tracer distributions of every conservative property will be linearly related to that of temperature in HILDA. This is obviously not the case in the real ocean. Can the low-latitude surface water be simulated as a mixed box for temperature? As seen from Fig. 3, the range of temperatures occurring in the LS region corresponds to nearly the full oceanic range, and the region can therefore certainly not be considered homogeneous with respect to temperature. Furthermore, the temperature distribution and the oceanic transport field, which is predominantly oriented along surfaces of constant density (isopycnals), are strongly correlated, as isothermals
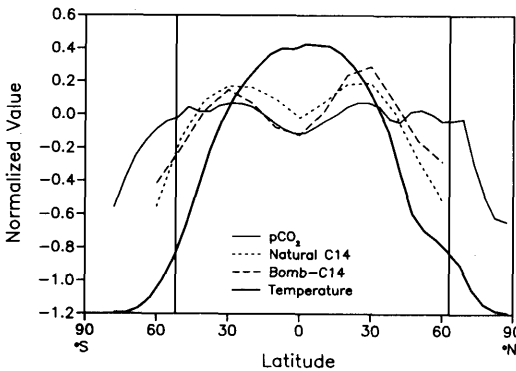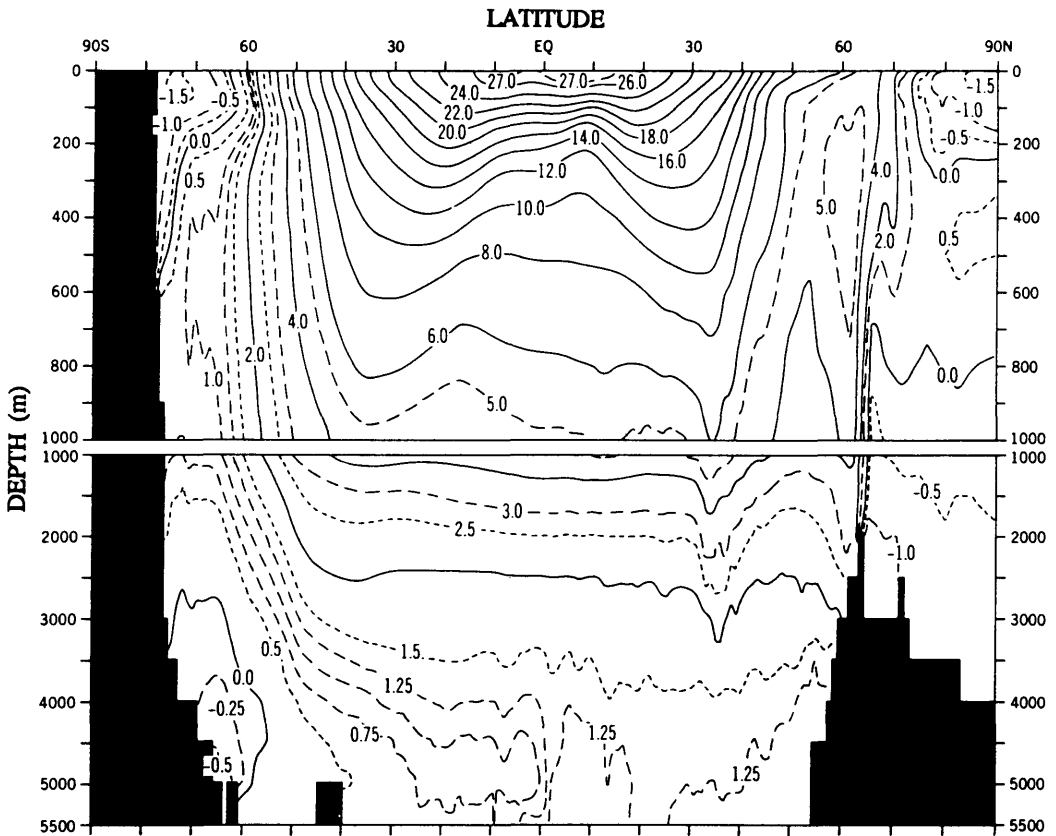
Fig. 4. Latitude-depth section of zonally averaged potential temperature versus latitude and depth in the world ocean (from Levitus, 1982). The isothermals approximately indicate the preferred transport paths for advection and mixing along isopycnal (constant-density) surfaces. The water warmer than the average LS temperature of 19.9 °C, occupying the latitude band 32 °S to 34 °N or 57 % of the total ocean surface area, is transported no deeper than 100–150 m by isopycnal transport.

and isopycnals nearly coincide. Fig. 4 shows the zonally averaged latitude-depth distribution of temperature in the world ocean, which at the same time approximately indicates the preferred transport paths for advection and mixing. The water warmer than 19.9 °C (average LS temperature), occupying the latitude belt 32 °S to 34 °N or 57 % of the total ocean surface area, is transported no deeper than 100–150 m by isopycnal transport. This shows that at depths $\geqslant 200$ m, the fraction of the water originating from the LS surface is considerably colder than the average LS temperature of 19.9 °C, because it stems from latitudes $>34°$ except for a relatively small fraction transported downwards by diapycnal mixing across isopycnal

surfaces. In the model, however, the temperature of all the water mixed down from the LS box is uniformly 19.9 °C. This explains why the sub-surface water is too warm in the BOMB and $K(z)$ models, although they correctly represent the downward penetration of bomb-^{14}C. (The problem is similar to that considered by Sarmiento and Rooth (1980) who discussed the difference between transport of radon escaping from the sediments and of buoyancy.)

A similar problem with temperature was also observed by Toggweiler et al. (1989b) in their 3-dimensional model study, their model thermo-cline being too warm. They attributed this to too strong downward mixing of heat by subgridscale

eddy diffusion, arguing in a similar way as we have done above concerning isopycnal mixing and latitudinal variation of surface temperature.

We conclude that HILDA (and other box models with similar horizontal resolution) is not appropriate for simultaneously simulating the distributions of ^{14}C and of temperature, because temperature varies significantly in the LS region, in contrast to ^{14}C. If HILDA is calibrated with temperature, as our version STST, then it can only yield reliable results for tracers whose concentrations are approximately linearly correlated to temperature, as for instance dissolved inert gases. The eddy diffusivity in version STST, determined using observed temperature, must obviously be rather small. Otherwise, downward mixing of warm surface water would be faster than the horizontal exchange of cold water between the HD box and the interior, and the Interior would be too warm. The problem is further discussed in Section 5 below.

We now turn to a detailed discussion of the distributions of ^{14}C. The too shallow penetration in version STST (Fig. 2c) indicates too low an eddy diffusivity K in the upper ocean, which is also documented by too low pre-industrial ^{14}C values in the upper 1500 m (Fig. 2b). This can also be expressed by stating that calibrations STST and BOMB span processes on different time scales. BOMB is appropriate for the penetration of a tracer from the atmosphere over a period of about a decade, whereas the STST calibration takes care of time scales of several hundred years, involving exchange with the deep ocean. Version $K(z)$ reconciles the two calibrations and can therefore be expected to be valid for time scales in the range (at least) from 10 to 10^3 years.

Validation of the high-latitude transport parameters indicates a problem. Based on an evaluation by Broecker et al. (1985), the average depth-integrated inventory of bomb-^{14}C for the HS plus HD region is $5.3 \cdot 10^9$ atoms cm^{-2} $(10 - 18 \cdot 10^9$ atoms cm^{-2} in the North Atlantic and $1 - 7 \cdot 10^9$ atoms cm^{-2} in the Southern Ocean), while we get considerably more for versions BOMB $(9.3 \cdot 10^9$ atoms cm$^{-2})$ and $K(z)$ $(8.7 \cdot 10^9$ atoms cm$^{-2})$. The relative error on the model inventory is $\pm 11\%$ (for version $K(z)$), obtained from a covariance analysis (Junkins, 1978) that considers the influence of uncertainties in the different transport parameters (cf. Table 1).

It is difficult to reconcile the small inventory of Broecker et al., with the model: even when the value for the vertical exchange rate u is reduced to zero, the HILDA inventory is still larger. The disagreement therefore might indicate a basic problem with the structure of our model, e.g., with the large-scale advection loop with upwelling in low and mid-latitudes, cf., Section 5. On the other hand, HILDA seems to reproduce the CFC inventories in high southern latitudes quite well (see below). The question therefore arises how accurate the evaluation method of the bomb-^{14}C inventories is for the Southern Ocean. A first source of uncertainty stems from the fact that data coverage in the Southern Ocean is rather sparse, with only 18 GEOSECS ^{14}C stations for the whole HS–HD region and very few reliable ^{14}C observations from pre-bomb time there. Second, Broecker et al., had to estimate the depth profile of bomb-^{14}C somewhat subjectively; for instance, they used tritium data for obtaining their inventories, assuming that tritium-free waters were also free of bomb-^{14}C. The choice of the depth where the water is tritium-free may have led to an underestimate of the inventories in the Southern Ocean. A sample calculation shown by Broecker et al., for a station at $55.0°$S, $50.1°$W indicates an estimated maximum penetration of bomb-^{14}C to 700 m depth only. However, CFCs are found all the way to the ocean bottom in Antarctic part of the South Atlantic (Warner, 1988; Weiss et al., 1990), with deep concentrations corresponding to 5–10% of the surface values. Thus, the evaluation method of Broecker et al., may underestimate the inventory in high latitudes. If their assessment method systematically misses, for instance, an average bomb-^{14}C contribution of $3°/_{oo}$ over a water column of 3000 m, this would correspond to a missing $1.5 \cdot 10^9$ atoms cm^{-2} in the inventory, compared to their total of $5.3 \cdot 10^9$ atoms cm^{-2}.

We have also calculated with HILDA, version $K(z)$, inventories of chlorofluorocarbons, the atmospheric concentrations of which have monotonously increased in the past about 50 years. In the past several years, CFC concentrations have been measured extensively in the ocean. The CFCs are purely anthropogenic, so that the data interpretation is not hampered by a background problem as with bomb-^{14}C. Our CFC model calculations were done in the context of the discussion about the potential effect on

atmospheric CO_2 of a large-scale fertilization of the Southern Ocean with iron, and we defined for that purpose the high-latitude region of HILDA (HS plus HD) as containing only southern hemisphere waters, approximately south of 46°S (Joos et al., 1991a, b). The solubility of CFC-11 is strongly temperature-dependent, and since the version $K(z)$ of HILDA yields too high temperatures in the low-latitude deep ocean, the calculated CFC-11 concentrations there are systematically wrong. We therefore only consider the high-latitude results here. For obtaining oceanic CFC inventories, we prescribed the atmospheric concentration history (M. Warner, personal communication) and calculated the invasion into the ocean, using solubilities of Warner and Weiss (1985) corresponding to the LS and HS model temperatures and gas transfer velocities for 7 m s^{-1} wind speed as given by Wanninkhof (1992) (14.2 and 7.9 cm h^{-1} for the LS and HS box, respectively). It is not very informative to compare the calculated CFC concentration in surface water with observations, because it is everywhere near equilibrium with the atmosphere (degree of equilibration in 1984: 98.4% for water in the LS box, 94.4% for the HS box). This is a contrast to ^{14}C and CO_2 for which there is, besides dissolved CO_2 gas, a large pool of dissolved inorganic carbon in ionic form, so that the equilibration time with the atmosphere is much longer than for the CFCs.

The model-calculated high-latitude inventory can be compared with observations. CFCs were measured during several expeditions between 1983 and 1985. From the data, we have obtained mean inventories by first calculating for each 5° latitude zone an average profile for all stations and then computing a weighted overall mean inventory, using as weights the ocean basin areas of 5° latitude bands. In the South Atlantic, CFC data are available from the AJAX experiment in 1983/84 (Warner, 1988; Weiss et al., 1990). The mean column inventory of CFC-11 for the 63 stations south of 46°S is 2000 (range of the 5° average inventories: 1440–2930) nmol m^{-2}. In the Pacific Ocean, an inventory of 2140 (1960–3045) nmol m^{-2} is obtained from data from the 1985 Wilkesland experiment (22 stations in the region 55° to 70°S, 145° to 165°E; R. F. Weiss and M. J. Warner, personal communication), and about 1850 (1500–2000) nmol m^{-2} for the region south

of 46°S and 150° to 170°W from data measured by NOAA-PMEL in 1984 (R. H. Gammon and D. Wisegarver, personal communication). The HILDA model result for 1984 is 1976 nmol m^{-2}, in excellent agreement with the observed inventories. The NOAA-PMEL cruise was repeated in 1990 (J. Bullister, personal communication); the mean inventory for the 14 stations is 2500 (2070–2840) nmol m^{-2}. The model yields a somewhat higher inventory of 3100 nmol m^{-2} for 1990.

Thus, the observed average high-latitude CFC-11 inventories agree well with the model result, in contrast to the bomb-^{14}C inventory. Since uptake of CFC is determined only by oceanic transport and not by gas exchange, this tends to support our choice of transport parameters. One might thus suppose that the bomb-^{14}C uptake is too large in the model because of inadequate gas exchange. In that case, one would expect that also surface ^{14}C levels are significantly too low, but this is not the case. We cannot explain the discrepancy in a definite way. The inventories are better defined for CFC-11 than for bomb-^{14}C (no background problem, more individual data), but the data coverage is incomplete also for CFC-11. We cannot rule out that the problem with bomb-^{14}C is due to inadequate representation of the high-latitude processes in HILDA, e.g., because deep-water formation in the North Atlantic and the Antarctic are not considered separately.

5. Apparent eddy diffusivities from 3-D model tracer fluxes

Eddy diffusion is used frequently in models for parameterizing large-scale vertical transport, but its use has been critically considered only by few authors. This is what we want to do in the following by discussing the processes which are parameterized by vertical eddy diffusion in models like HILDA. These include not only local mixing, but also the transport by large advection cells which form sub-grid scale processes in the coarse-resolution models. In this context, we will address the problem that vertical eddy diffusivities estimated for local mixing processes (e.g., Gargett, 1976 and 1984, Garrett, 1979) are often considerably smaller than the values we and other authors have derived from large-scale tracer distributions.

Turbulent diffusion can be introduced for time-

varying flow by separating the velocity $v(t)$ and the concentration $c(t)$ of some quantity into a time-average and a fluctuating part (see, e.g., Pond and Pickard, 1983), according to:

$$v(t) = \bar{v} + v'(t), \qquad c(t) = \bar{c} + c'(t), \qquad (3)$$

In our case, $v(t)$ is the vertical velocity. An overbar indicates an average over a chosen time interval. The time-average tracer flux (per unit area) is then given by

$$\overline{vc} = \bar{v}\bar{c} + \overline{v'c'} \qquad (4)$$

where the first term to the right is the transport by the mean advection $\bar{v}$ and the second term gives the turbulent (eddy) flux. This turbulent flux corresponds to local mixing. In contrast, in advective-diffusive models, the averaging is done not only over time, but also over some space region. For the HILDA model, the averaging region is a surface of constant depth extending over the Interior region. An analogous separation as above can be performed (Newell, 1963), now for the time-average quantities into a space-average part and a part fluctuating in space (in our case a function of latitude and longitude):

$$\bar{v} = \langle \bar{v} \rangle + \bar{v}^*, \qquad \bar{c} = \langle \bar{c} \rangle + \bar{c}^*, \qquad (5)$$

where $\langle \ \rangle$ denotes a space-average and $*$ the spatial fluctuation (deviation from the horizontally averaged value at a given depth). Hence, the time- and space-average flux F is:

$$F \equiv \langle \overline{vc} \rangle = \langle \bar{v} \rangle \langle \bar{c} \rangle + \langle \bar{v}^* \bar{c}^* \rangle + \langle \overline{v'c'} \rangle. \qquad (6)$$

The average vertical flux thus consists of a transport by the mean advection $\langle \bar{v} \rangle$, a transport by the spatial fluctuations of the time-average circulation, that is by standing eddies $\bar{v}^*$, and a transport by transient eddies.

The eddy diffusion approach consists in assuming that the turbulent flux (last two terms in eq. (6)) is proportional to the mean tracer gradient. This corresponds to the picture of ocean mixing by many sub-grid scale eddies, exchanging water parcels between regions of high and regions of low concentration. Eq. (6) then becomes

$$F = \langle \bar{v} \rangle \langle \bar{c} \rangle - K_{app} \left\langle \frac{\partial \bar{c}}{\partial z} \right\rangle, \qquad (7)$$

where K_{app} is an apparent eddy diffusivity.

For studying the parameterization of large-scale mixing by eddy diffusion, we have followed and expanded the approach of Sarmiento (1983), who calculated apparent vertical eddy diffusivities K_{app} for tritium in the North Atlantic from model-calculated vertical tracer fluxes. In the low-latitude Interior reservoir of HILDA, vertical tracer transport occurs by advection and eddy diffusion. We performed an analysis in terms of apparent diffusion and advection, taking the v and c fields from the simulations of natural radiocarbon and temperature with a 3-dimensional Cox-Bryan ocean model by Toggweiler et al. (1989a; their model version P). We consider the vertical tracer transport due to water circulation within the 3-D model region corresponding to the Interior reservoir in HILDA, that is beneath sea surface temperatures of $>5°C$. Only advection is taken into account, but not transport by explicit diffusion and by convection in the 3-D model.

The contribution of transient eddies, $\langle \overline{v'c'} \rangle$, to the turbulent flux corresponds to the spatial average of local mixing, which seems to be small for the 3-D ocean model. (Due to its limited resolution, a numerical model can anyhow not simulate the small-scale mixing due, e.g., to breaking internal waves.) Therefore, we neglect this term. Then, the turbulent transport F_{eddy} equals the contribution of spatial fluctuations:

$$F_{eddy} = \langle \bar{v}^* \bar{c}^* \rangle = A^{-1} \int \bar{v}^* \bar{c}^* \, dA, \qquad (8)$$

where the integration extends over a horizontal area A in the region corresponding to the Interior domain in HILDA. Combining eqs. (6) to (8) we get

$$K_{app} = \frac{\langle \bar{v}^* \bar{c}^* \rangle}{\partial \langle \bar{c} \rangle / \partial z} = \frac{\langle \bar{v} \rangle \langle \bar{c} \rangle - \langle \overline{vc} \rangle}{\partial \langle \bar{c} \rangle / \partial z}. \qquad (9)$$

The space-average values $\langle \bar{v} \rangle$, $\langle \bar{c} \rangle$ and $\langle \overline{vc} \rangle$ were calculated from the 3-D model results for $\bar{v}$ and $\bar{c}$, i.e., from the time-average values at the 3-D model grid points, provided by R. Toggweiler (personal communication). $\langle \bar{v} \rangle$ corresponds to $-w$, the negative upwelling velocity, in HILDA.

The resulting apparent eddy diffusivities for steady-state ^{14}C and temperature are shown in Fig. 5. Due to weak gradients of temperature and ^{14}C, K_{app} is not well defined below 1000 to 2000 m,
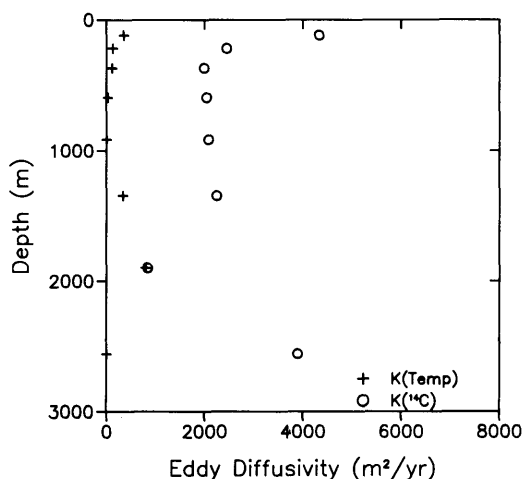
Fig. 5. Apparent eddy diffusivities K_{app} as calculated from the distributions of steady-state ^{14}C and temperature obtained by Toggweiler et al. (1989a) using a 3-D General Circulation Model.

and in fact, we even get negative values (plotted as 0 in Fig. 5) at some depth levels. Negative K_{app} values may arise because the tracer distribution, and therefore the concentration gradient, in the considered region is not due solely to vertical transport, as implicitly assumed in our discussion, but also to lateral fluxes. In the uppermost 500–1000 m, the K_{app} values for ^{14}C are roughly 2000 to 4000 m yr^{-1}, agreeing in order of magnitude with the eddy diffusivities determined for HILDA versions BOMB and $K(z)$ and significantly larger than the values determined theoretically and experimentally for small-scale vertical mixing (Garrett, 1979).

We have found above that in the HILDA model, the eddy diffusivity has to decrease with depth in order that natural as well as bomb-^{14}C can be simulated well. In the top 1000 m, the apparent eddy diffusivities for ^{14}C and for temperature are highest at the surface and then decrease with depth (Fig. 5), in qualitative agreement with our assumption for the $K(z)$ version. This correspond to more vigorous tracer transport in the upper water layers by the wind-driven and the thermohaline circulation. The quantitative agreement between the K_{app} values and the HILDA eddy diffusivities is not good, but this is not expected considering the schematic way in which the depth dependence of the model eddy diffusivity was chosen and in

view of the fact that HILDA was calibrated using observations and not the 3D model output.

K_{app} values from temperature are 100–800 m^2 yr^{-1} (Fig. 5), considerably lower than those obtained from natural ^{14}C. The difference can be explained by our above arguments in connection with the HILDA eddy diffusivities, involving the correlation between vertical velocity and the tracer distribution. The turbulent flux $\langle \bar{v}^* \bar{c}^* \rangle$ corresponds to a spatial correlation of the velocity and the concentration fields (cf. eq. (8)). While the space dependence of the standing-eddy field, $\bar{v}^*$, is the same for all tracers, the space dependence of the concentration anomalies, $\bar{c}^*$, depends on the tracer. In Fig. 3, $\bar{c}^*$ is shown as a function of latitude for surface observations of natural and bomb-produced ^{14}C, excess CO_2 and for temperature. The latitude dependence of $\bar{c}^*$, and therefore the spatial correlation $\langle \bar{v}^* \bar{c}^* \rangle$, are similar for the first three tracers, and therefore similar K_{app} value must apply. Temperature has a rather different latitude dependence than the other three tracers (Fig. 3), which leads to different K_{app} values. The fact that relatively small K_{app} values are found for temperature can be understood when considering the whole world ocean. In a steady state, the global vertical heat flux is zero, but the vertical temperature gradient does not vanish. According to eq. (9), this corresponds to $K_{app} = 0$ (the global mean advection velocity is of course zero). Obviously, the basic assumption of the eddy diffusion concept, that a tracer gradient drives a flux, is not valid for the large-scale oceanic temperature distribution. This is so because the global temperature distribution is not the result of turbulent transport by many eddies, but of the thermohaline circulation which essentially consists of one global advection cell.

In summary, the evaluation of the 3-D model transports of ^{14}C in the frame of the geometry of HILDA leads to similar values for the eddy diffusivity as obtained when calibrating HILDA with the observed ^{14}C distribution. Qualitatively, this evaluation also confirms our HILDA result that the eddy diffusivity has to decrease with depth in the upper layers of the ocean. This depth dependence is contrary to that expected from an inverse relation with the stability of the water column, which has been expected based on theoretical arguments (Welander, 1968; Gargett, 1984) and found experimentally for tracer-derived

eddy diffusivities (Sarmiento et al., 1976); from these results, a small diffusivity would be expected at the top of the thermocline and large values in the deep sea (Hoffert, 1989). Welander's study deals with local mixing, while in HILDA and similar global ocean models, eddy diffusion represents a parameterization of very large circulation cells as sub-grid processes (the Interior reservoir of HILDA has a meridional extension of roughly 10,000 km), which are most vigorous near the surface. Clearly, the value of an eddy diffusivity depends on the spatial scale, i.e., on the horizontal area over which the spatial averaging is performed.

We note furthermore that temperature, and therefore any property that is strongly correlated with temperature, as for instance oxygen, is not well reproduced in HILDA by the calibration based on natural and bomb-produced ^{14}C. The HILDA geometry is appropriate for ^{14}C and for anthropogenic CO_2, which have roughly constant values in the LS region, but not for temperature.

The procedure for calculating K_{app} also yields average advection velocities $\bar{v}_z$ for the region of the 3-D model of Toggweiler et al. (1989a) which corresponds to the HILDA Interior reservoir. In contrast to HILDA where we have obtained upwelling in low latitudes (w positive), this average advection velocity $\bar{v}_z$ in the 3-D model is downward at all depths except at the lowest model layer, with absolute values of about 2.5 m yr^{-1} near the surface and decreasing downward. In the 3-D model, the thermohaline circulation does not involve a homogeneous vertical advection in mid- and low latitudes, but has a cellular structure with a strong deep circulation cell between about 40° S and 65° S. This cell consists of an upward transport in the high southern latitudes of more than $20 \cdot 10^6$ m^3 s^{-1} of water, which then downwells north of 50° S; i.e., the cell is cut across by the surface 5°C isothermal forming the low-to-high latitude boundary in HILDA. In northern high latitudes, North Atlantic Deep Water (NADW) is formed at a rate of about $15 \cdot 10^6$ m^3 s^{-1}, but part of the NADW formation occurs farther south than the LS–HS boundary. Thus, magnitude and sign of the average vertical velocity in the 3D-model region including the low and mid-latitudes depend critically on where precisely the poleward boundaries of this region are chosen. Nevertheless, it is interesting that in the 3-D model, the *average* vertical velocity is upward in the region south of about

52° S and downward between 52° S and 63° N, in contrast to the often-made assumption of a more or less uniform upwelling motion in low latitudes. This may also be correct for the real ocean: Broecker et al. (1985) concluded, based on small inventories of bomb-^{14}C in high southern latitudes, that there is large-scale upwelling in the Southern Ocean, which conforms to the average 3-D advection field. In HILDA, we have upwelling in the Interior (positive w), but the value of w is so small (<1 m s^{-1}) that a change of sign would not significantly affect the model results.

6. Atmospheric CO_2 increase in the past two centuries

6.1. Modelling considerations

For studying the oceanic CO_2 uptake, we assume, as has mostly been done in similar work, that the natural carbon cycle processes were in steady state before the onset of the man-made perturbation and have continued to operate unchanged since. In this case we can consider only perturbations in the model; in particular, we can neglect the influence of marine biology. Formally, we consider only perturbations in the model equations for CO_2, defined as the difference in concentration between time t and pre-industrial time. These equations can be looked upon as the difference between the full equations for time t and for pre-industrial time. For isotopes, total concentrations of the isotopic molecules are considered; for this purpose, we assume a constant pre-industrial ΣCO_2 concentration of 2.053 mol m^{-3} in seawater, in equilibrium with a constant atmospheric CO_2 concentration of 280 ppm (278.3 ppm for the deconvolution, see below). The model equations are analogous to those given by Siegenthaler (1983) for the box-diffusion and outcrop-diffusion models.

The net air-to-sea flux of CO_2 is driven by the difference between atmospheric CO_2 concentration and surface-water pCO_2. Thus, for calculating the oceanic CO_2 uptake, we have to relate the changes in pCO_2 with those in the concentration of dissolved inorganic carbon (ΣCO_2) in sea water. For this purpose, we have developed a simple function relating δpCO_2 to $\delta \Sigma CO_2$, where δ denotes the perturbation, i.e., the change since pre-industrial time: $\delta pCO_2 = pCO_2 - pCO_{2,0}$; we take

$pCO_{2,0} = 280$ ppm. From the equations governing the chemical equilibria of the carbonate system (Bacastow, 1981), we obtained the following relation, using the Lyman dissociation constants for carbonic acid (Takahashi et al., 1976) and the CO_2 solubilities of Weiss (1974) and assuming a salinity of 35 psu and a constant alkalinity of 2300 μeq kg^{-1}:

$$\delta pCO_2 = \frac{z_0 \, \delta \Sigma CO_2}{1 - z_1 \, \delta \Sigma CO_2}, \qquad (10)$$

with

$$z_0 = 1.7561 - 0.031618T + 0.0004444T^2,$$

$$z_1 = 0.004096 - 7.7086 \cdot 10^{-5}T + 6.10 \cdot 10^{-7}T^2, \qquad (11)$$

where T is in °C, δpCO_2 in ppm and $\delta \Sigma CO_2$ in μmol kg^{-1}. Eqs. (10, 11) approximate the exact calculation to better than 1 % for $0°C \leqslant T \leqslant 30°C$ and $\delta pCO_2 \leqslant 200$ ppm. This function has also been used for a 3-D ocean carbon cycle model by Sarmiento et al. (1992). For HILDA, we have evaluated eqs. (10, 11) for the temperatures of the LS and HS boxes and, for use in the gas exchange equations, calculated buffer factors ξ, defined as

$$\xi = \frac{\delta pCO_2}{pCO_{2,0}} \frac{\Sigma CO_{2,0}}{\delta \Sigma CO_2}. \qquad (12)$$

We have later also carried out calculations using the formulation for the carbonate chemistry given by Peng et al. (1987), which includes carbonic acid dissociation constants of Mehrbach et al. (1973) and the influence of boric, silicic and phosphoric acid. The results for the perturbations agreed with the ones using the other buffer factors within 0.1 to 0.5 %.

The buffer factor is greater for cold than for warm seawater, so that at chemical equilibrium, a given atmospheric CO_2 perturbation corresponds to a smaller ΣCO_2 change in cold water than in warm water and one liter of cold seawater takes up less additional CO_2 than one liter of warm water.

6.2. CO_2 simulations and comparison of different models

We have run two scenarios for the anthropogenic CO_2 perturbation. The *first* one corresponds to a deconvolution of the atmospheric CO_2 concentration history as given by ice core data and, after 1958, by direct atmospheric measurements, in the same way as carried out using the box-diffusion and the outcrop-diffusion models by Siegenthaler and Oeschger (1987). In the model, we prescribe the observed data for the atmosphere and calculate the flux into the ocean. The response of the terrestrial biosphere is not explicitly simulated in the model. The sum of the annual increase of the CO_2 mass in the atmosphere (observed) and the ocean (calculated by the model) is set equal to the net input into the atmosphere plus ocean system. In this way, an estimate is obtained for the total annual CO_2 production rate, which is due to combustion of fossil fuels plus deforestation minus a potential land biospheric sink, due, e.g., to fertilization by the increased levels of atmospheric CO_2 and nutrients, plus/minus any other sources or sinks. The total production rate minus the fossil production rate (Rotty and Masters, 1985; Marland, 1989) yields the non-fossil flux which probably corresponds to the net biotic contribution. The *second scenario* consists in prescribing the fossil CO_2 production rate as model input and calculating the resulting
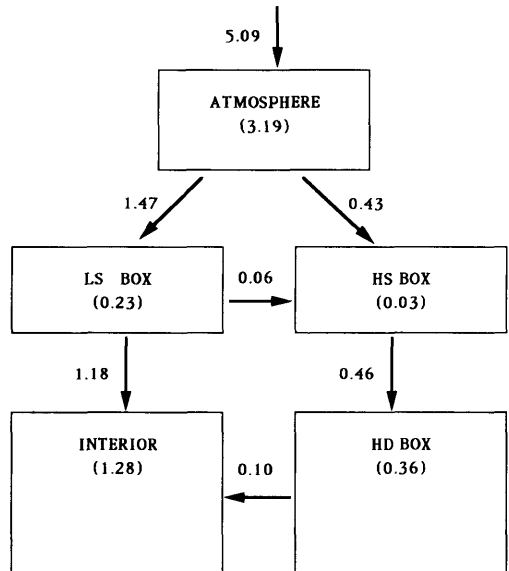

Fig. 6. Fluxes of perturbation CO_2 (in Gt C yr^{-1}) between the different model reservoirs in 1980, obtained from the deconvolution using model version $K(z)$.

atmospheric concentration increase, starting at an initial value of 280 ppm. This scenario is not realistic in that it neglects the emissions from deforestation, but it is considered here for comparison, since many model studies have been performed in this way. We have carried out CO_2 simulations using all three versions of HILDA, but we will concentrate below on version $K(z)$ as the most appropriate. Before discussing the significance of the results, we now consider modelling aspects of the results and compare the different models.

Fig. 6 shows the CO_2 fluxes between the different model reservoirs in 1980 as obtained from the deconvolution. 23% of the net flux invading the ocean enter via the high latitude surface, although its area is only 16% of the global ocean surface. The reason is that in high latitudes, surface water laden with excess CO_2 is faster transported to depth than elsewhere. In 1980, the pCO_2 increase in the low-latitude surface box is 52.3 ppm, and 48.1 ppm in the high-latitudes, compared to the atmospheric increase of 59.8 ppm; the ratio of the air-to-sea fluxes per m^2 is therefore $(59.8 - 48.1)/(59.8 - 52.3) = 1.56$. Note that we assume the same gas exchange coefficient at all latitudes.

Results from the $K(z)$ and BOMB runs and from three other model studies are compared in Table 3, which contains fluxes for 1980, cumulative perturbations and airborne fractions. We define the airborne fraction as ratio of atmospheric increase to total calculated or prescribed CO_2 production in a given period. For the deconvolution (version $K(z)$), the airborne fraction for the period 1770–1980 is 0.542 ± 0.015; the indicated error, obtained

Table 3. *Model results for anthropogenic CO_2 increase for HILDA versions $K(z)$ and BOMB, for the (bomb-^{14}C calibrated) box-diffusion and outcrop-diffusion models (Siegenthaler and Oeschger, 1987) and for the 3-dimensional ocean carbon model of Sarmiento et al. (1992)*

	HILDA $K(z)$	HILDA BOMB	Box-Diffusion	Outcrop-Diffusion	3-D
Fluxes for 1980 (Gt C yr^{-1}) for the deconvolution					
fossil CO_2 production rate	5.26	5.26	5.28	5.28	5.24
non-fossil production rate	−0.22	0.09	0.10	1.18	−0.48
atmospheric increase	3.11	3.11	3.13	3.13	3.09
oceanic uptake	1.93	2.16	2.25	3.33	1.67
Perturbations 1770–1980 (Gt C)					
fossil production	162	162	163	163	162
Deconvolution:					
non-fossil production	72	88	88	153	56
atmosphere (observed)	127	127	128	128	127
oceanic uptake	107	123	123	188	92
Only fossil CO_2 input:					
atmosphere (calculated)	101	97	99	84	105
oceanic uptake	61	65	64	79	60
Airborne fraction					
Deconvolution:					
1770–1980	0.542	0.508	0.511	0.406	0.582
1959–1983	0.611	0.581	0.581	0.479	0.642
Only fossil CO_2 input:					
1770–1980	0.619	0.599	0.612	0.519	0.638
1959–1983	0.635	0.615	0.625	0.533	0.666

Results are given for the deconvolution of the Siple/Mauna Loa data as well as for runs using the emissions from fossil fuel combustion as model input.

from a covariance analysis, corresponds to the uncertainties in the model parameters stemming from the calibration (see Table 1). The oceanic uptake in the same period is 107 Gt C $\pm$ 5.9%.

For version BOMB of HILDA, the oceanic CO_2 uptake is about 10% larger than in version $K(z)$ (Table 3). In the latter version, the eddy diffusivity is higher at the top of the Interior reservoir, but then decreases rapidly with depth: at levels deeper than 140 m below the top of the Interior reservoir, the $K(z)$ eddy diffusivity is smaller than the BOMB value of 4700 m. For depth-independent K, the mean penetration depth of anthropogenic CO_2 is given by $\sqrt{K\tau}$ (Oeschger et al., 1975), where $\tau \approx 30$ yr is the approximate e-folding time of the anthropogenic production rate. For version BOMB, this mean penetration depth is 375 m, so that the bulk of the perturbation is transported downward faster in this model version (as it feels a higher eddy diffusivity) than in version $K(z)$. As a consequence, the concentration of perturbation CO_2 for version $K(z)$ is slightly larger than for version BOMB near the surface, but smaller at lower levels (see Fig. 7), which explains the difference between the two results. Version STST has a lower oceanic uptake, 82 Gt C from 1770 to 1980, compared to 107 Gt C for $K(z)$, obviously

because of the smaller eddy diffusivity. We shall not discuss version STST further, because we consider its vertical exchange in the upper part of the low-latitude ocean as too slow.

The results for version BOMB are very similar to those for the bomb-calibrated box-diffusion model of Siegenthaler and Oeschger (1987) (cf. Table 3), while one might expect that the HILDA ocean would take up more CO_2 because of the rapid circulation in high latitudes. However, the box-diffusion model was calibrated using a higher inventory of bomb-^{14}C and correspondingly mixes faster than HILDA. The oceanic uptake is larger for the outcrop-diffusion model than for all others, because in that model, CO_2 that has entered high-latitude oceanic outcrop is immediately mixed into the deep sea, so that the simulated flux into the ocean must be unrealistically large. The 3-D model of Sarmiento et al. (1992) yields less oceanic uptake than the simple models listed in Table 3. This 3-D model ocean has too small an uptake of bomb-^{14}C into the thermocline (Toggweiler et al., 1989b), so that it probably also underpredicts the CO_2 uptake somewhat. The results of a deconvolution carried out by Keeling et al. (1989a, Fig. 46) using the 3-D ocean model of Maier-Reimer and Hasselmann (1987) seem to be comparable to those from HILDA, version $K(z)$. The calculated oceanic CO_2 uptake is therefore similar for all models in Table 3, except for the outcrop-diffusion model which clearly yields too large oceanic fluxes.

From Table 3, we note that the airborne fraction is smaller for the whole period 1770–1980 than for the recent time span, 1958–1983. The reason is that the penetration depth into the ocean becomes larger the longer the characteristic time τ of the CO_2 increase is. For the period 1958–1983, τ is shorter (the production grew faster) than for the whole period 1770–1980, because of the considerable input which occurred, according to the deconvolution calculations, a long time ago in the 19th century. The CO_2 emitted in the 19th century has therefore had much time to penetrate to deeper layers of the ocean. For the same reason, the airborne fraction calculated for a pure fossil-fuel CO_2 source is larger (the oceanic uptake is smaller) than for the deconvolution. The difference between the two scenarios (i.e., the dependence on τ) is smaller for version $K(z)$ than BOMB, which is due to the fact that in contrast to version BOMB, the $K(z)$ eddy diffusivity decreases with depth, so that
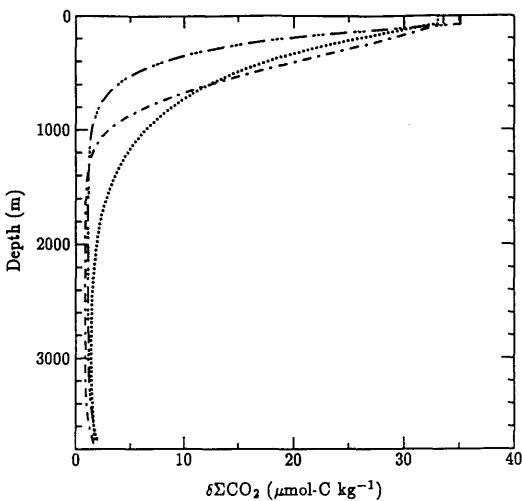

Fig. 7. Calculated vertical profiles of $\delta\Sigma CO_2$, the concentration of perturbation carbon in the low-latitude reservoirs, in 1974 for the deconvolution of the combined Siple-Mauna Loa data. Model versions: $\cdots\cdots - \cdots - \cdot$ STST, $\cdots\cdots$ BOMB, $-\cdot-\cdot$ $K(z)$.

the penetration of a perturbation is at first rapid near the surface, but then becomes rather slow when the perturbation has reached a few 100 m depth (see also Fig. 10).

The dependence on the characteristic time is illustrated for different models by the atmospheric response to a production pulse that corresponds to
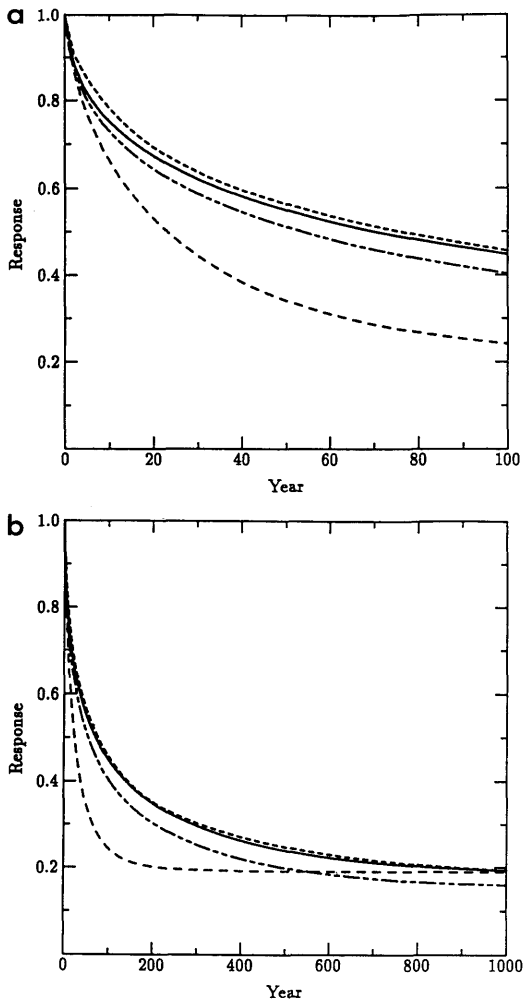

100% of the pre-industrial carbon mass (Fig. 8). This is a small enough perturbation that the non-constancy of the buffer factor is not yet important. Not surprisingly, the outcrop-diffusion model curve is the lowest of all, while the other three models have similar pulse responses. The response function of version $K(z)$ is nearly identical to that of the box-diffusion model during the first 10 years; later, it is larger (smaller oceanic uptake). The atmospheric response is somewhat higher for the 3-D model of Sarmiento et al. (1992) than for HILDA, particularly in the first few decades, in agreement with the higher airborne fractions (Table 3). In general, however, these two models are remarkably similar over the whole range from 0 to 1000 years. This indicates that HILDA, version $K(z)$, simulates the time dependence of the CO_2 uptake by the 3-D Cox-Brian General Circulation Model rather well over different time scales. By performing a suitable calibration of HILDA (for instance using the 3-D model-generated oceanic bomb-^{14}C distribution of Toggweiler et al., 1989b), the resemblance of the two response functions could possibly be made even closer, so that HILDA could then be used as a simple substitute for the 3-D model for calculating atmospheric CO_2 scenarios. After 1000 years, the airborne fractions of the different models are between 16 and 20%, which approximately reflects the equilibrium partitioning of the excess CO_2 between atmosphere and ocean. The value is smaller for the box-diffusion model than for all others for a reason that will immediately become evident.

Fig. 9 shows the fluxes from the atmosphere into the HS and LS boxes after the pulse input for version $K(z)$. The fluxes are initially very high (at $t = 0$: 54.80 Gt yr^{-1} into the LS box, 10.44 Gt C yr^{-1} into the HS box), but then decay very quickly because pCO$_2$ in surface water increases strongly within a few years. In the first 100 years, the low-latitude flux dominates because of the larger area, but as the gradient in the upper Interior reservoir and therefore the downward diffusive transport decreases, the high latitudes become more and more important as a CO_2 sink. After many centuries, a new steady state is approached. The high latitude ocean then releases CO_2 to the atmosphere, because the buffer factor is higher there than in the LS box; the atmospheric transport is compensated by a flow of perturbation CO_2 from
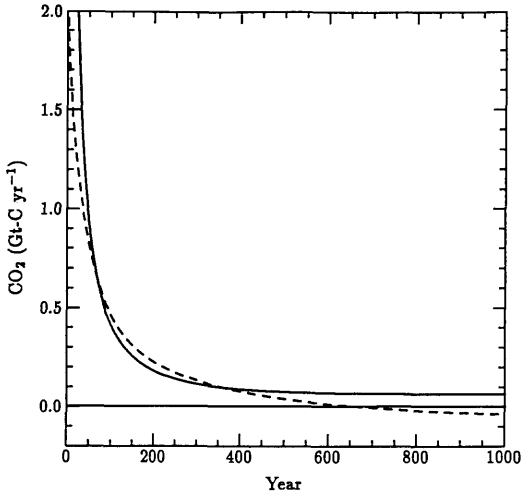
Fig. 8. Response of the atmospheric CO_2 concentration to a pulse input at time $t = 0$, corresponding to 100% of the preindustrial CO_2 amount, for different carbon cycle models. The initial value is set to 1. Line signatures: —— HILDA, version $K(z)$; – – –: 3-D Ocean General Circulation Model (Sarmiento et al., 1992); — — — — box-diffusion model; — — — — outcrop-diffusion model (the latter two both from Siegenthaler and Oeschger, 1987). Figs. 8a and 8b only differ in the time scale.

Fig. 9. CO$_2$ fluxes from the atmosphere to the low-latitude ocean (solid line) and the high-latitude (dashed line) ocean boxes (HILDA version $K(z)$) after a pulse input into the atmosphere corresponding to 100% of the preindustrial atmospheric carbon mass.

the LS box (high additional ΣCO_2) via the deep ocean to the HS box (low additional ΣCO_2). This phenomenon does of course not occur in the purely one-dimensional box-diffusion model, which also explains why the atmospheric CO$_2$ level after 1000 years is lower in this model than in the others.

6.3. Model-calculated fluxes and the global CO$_2$ balance

Fig. 10 shows the CO$_2$ fluxes for the deconvolution scenario according to version $K(z)$ of HILDA. The general result is similar as obtained by Siegenthaler and Oeschger (1987), Keeling et al. (1989b) and Sarmiento et al. (1992) who performed the same kind of deconvolution using different models, and also to that of Enting and Pearman (1987). From before 1800 on, a relatively large CO$_2$ production rate is found throughout the 19th century, while significant use of fossil fuels began only in the late 19th century. This general result does not depend on the model used; it is implied by the ice core CO$_2$ data which indicate an atmospheric increase from the late 18th century to 1900 by about 17 ppm or 36 Gt C, while the cumulative fossil production until 1900 amounted to only 12 Gt C. Provided the ice core data are a
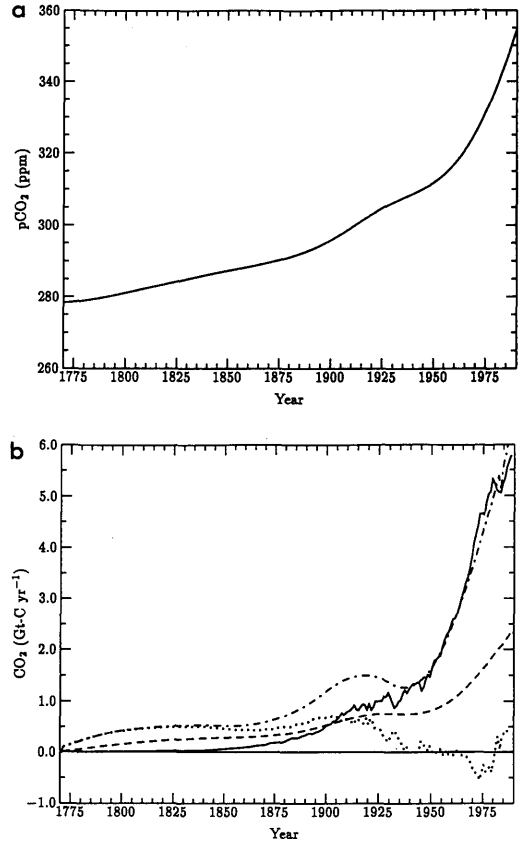

Fig. 10. Result from a model deconvolution of the atmospheric CO$_2$ concentration history according to the combined Siple ice core/Mauna Loa data (top figure; Neftel et al., 1985; Friedli et al., 1986; Keeling et al., 1989a). The deconvolution yields the total production rate (dash-dotted). The non-fossil production rate (total-fossil, dotted) corresponds to the net contribution (emissions-uptake) from the terrestrial biota. The fossil CO$_2$ production (solid) is taken from Rotty and Masters (1985) and updated by Marland (1989). Dashed: oceanic uptake.

true record of atmospheric CO$_2$ levels and considering that the ocean must have taken up an amount of excess CO$_2$ comparable to that in the atmosphere, it is clear that a significant non-fossil source existed in the 19th century.

From about 1940 on, the calculated non-fossil production rate is near or below zero until 1980 (Fig. 10). This result, which has also been found using other models (cf. Table 3), is in marked contrast to the estimates of emissions from

deforestation and changed land use, which yield a general increase during this century with values between 0.6 and 2.5 Gt C yr^{-1} for 1980 (IPCC, 1990). As discussed in the papers mentioned above, this suggests that either a large terrestrial sink exists, connected with carbon uptake by land biota, or that the ocean-atmosphere models are in error, or that the basic assumption of all these model studies (that the natural part of the oceanic carbon cycle has operated in a steady-state way before and since the industrialization) is not valid. The latter possibility seems not very likely in view of the fact that ice core CO_2 data from the South Pole indicate a rather stable atmospheric CO_2 level in the millenium preceding industrialization (Siegenthaler et al., 1988).

The four models of Table 3 (excluding the out-crop-diffusion model) yield a net oceanic CO_2 uptake in 1980 between 1.6 and 2.1 Gt C yr^{-1}, with the HILDA $K(z)$ result in the middle of this range. This is in clear contrast to the conclusion of Tans et al. (1990), who stated, based on the evaluation of atmospheric CO_2 data and oceanic pCO_2 observations using a 3-D atmospheric tracer transport model, that the oceanic uptake during 1980–1987 was at most 1 Gt C yr^{-1}. Keeling et al. (1989b), who performed a similar analysis, obtained an oceanic sink of 2.2 Gt C yr^{-1}. Both groups of authors concluded that there must exist

a rather large sink for anthropogenic CO_2 in the Northern Hemisphere. Tans et al. attributed this sink to the continents (based on the oceanic pCO_2 data), while Keeling et al., attributed it to the North Atlantic Ocean, based on atmospheric $^{13}C/^{12}C$ measurements. Our model study as well as others clearly favour the oceanic sink.

7. Anthropogenic perturbation of the carbon isotopes

Since fossil fuels contain no ^{14}C and fossil fuels as well as biomass have a lower $^{13}C/^{12}C$ ratio than atmospheric CO_2, the man-made perturbations have also led to a change in the isotopic composition of atmospheric CO_2 (Suess effect). For studying these perturbations, a simple land biosphere box that exchanges carbon with the atmosphere was added. Its pre-industrial size is 1200 Gt C i.e., about twice as much as the pre-industrial atmosphere, and the mean residence time for carbon is 20 years. These biospheric parameters were chosen such that the 1-box biosphere has a roughly similar isotope pulse response function as the 4-box biosphere used by Siegenthaler and Oeschger (1987) in combination with the box-diffusion model. We assume that the non-fossil production calculated by means of the

Table 4. *Isotopic perturbations obtained from the deconvolution of the Siple/Mauna Loa data for HILDA version $K(z)$, for the box-diffusion (BD) model (Siegenthaler and Oeschger, 1987) and as observed (where appropriate observations are available)*

Shift of $\delta^{13}C$ ($^o/_{oo}$)	HILDA $K(z)$	BD	Observation
atmosphere (1770–1980)	−1.29	−1.19	−1.14 ± 0.15[1]
LS box (1770–1970)	−0.68	−0.46[a]	−0.4 to −0.5[2]
HS box (1770–1970)	−0.39		
Shift of $\Delta^{14}C$ ($^o/_{oo}$) 1860–1950:			
atmosphere	−20.4	−17.8	−17[3]
LS box	−6.8	−4.7[a]	−6 to −12[4]
HS box	−2.7		

[a] The values for the BD model are for the mixed layer and can be compared to an area-weighted mean for LS and HS.

[1] Friedli et al. (1986).

[2] Nozaki et al. (1978); Druffel and Benavides (1986).

[3] Stuiver and Quay (1981).

[4] Druffel and Suess (1983).

deconvolution is of biospheric origin and has the corresponding isotopic composition. $^{13}C/^{12}C$ ratios of the emissions from fossil fuel use are taken from Tans (1981). Table 4 shows the results for version $K(z)$ (those for BOMB are very similar), together with results for the box-diffusion model (Siegenthaler and Oeschger, 1987) and observed values. The changes predicted by HILDA are slightly larger than the observed ones, but still compatible with them within the experimental errors. The HILDA results are also somewhat larger than those from the box-diffusion model. One possible explanation for this difference is that we used a smaller inventory of bomb-^{14}C to calibrate the HILDA model than was used for calibrating the box diffusion models, so that vertical oceanic mixing as well as the gas exchange are slower. The difference might also be due to the different biospheric submodels used. In order to test the influence of the biosphere, we carried out a simulation without land biosphere. This has no influence on the CO_2 increase, but on the isotopic changes (Suess effect) in the atmosphere. The resulting $^{13}C/^{12}C$ change from 1770 to 1980 is $-1.60°/_{oo}$ instead of $-1.29°/_{oo}$ with a biosphere, the ^{14}C change from 1960 to 1950 is $-35.1°/_{oo}$ instead of $-20.4°/_{oo}$. This demonstrates that the isotopic signal is diluted not only by exchange with the ocean, but also with the biosphere. A deeper study of the Suess effect would therefore have to consider the biospheric submodel in more detail.

8. Conclusions

HILDA includes the effect of deep-sea ventilation via the outcrop in high latitudes and is thus nearer to reality than a purely one-dimensional model, while still retaining a simple structure. The model has been calibrated using the distributions of natural as well as of bomb-produced ^{14}C. We find that in order to simulate both distributions, governed by processes on time scales ranging between 10 and 1000 years, it is necessary to introduce a depth-dependent eddy diffusivity. This also seems appropriate from an oceanographic standpoint, since vertical exchange is more vigorous in the top few 100 m than in the deep sea due to the wind-driven as well as the thermohaline circulation. Apparent eddy diffusivities derived from the results of a 3-D Ocean General Circula-

tion Model agree in order of magnitude with those determined for the upper ocean in HILDA. The HILDA model cannot simultaneously reproduce the oceanic distributions of bomb-^{14}C and of temperature, because temperature varies strongly over the model's low-latitude surface box and thermocline waters at different depth are ventilated from surface regions with considerably different temperatures. In contrast, the concentration of tracers like ^{14}C or anthropogenic CO_2 does not vary as strongly as temperature with latitude in the LS region, so that lumping the latitude belt between about 52°S and 63°N into a single surface box seems permissible for these tracers. The simulated inventory of bomb-^{14}C in the Southern Ocean appears to be too large, but the inventory of CFC-11 agrees well with available observations. The reason for this discrepancy is difficult to identify. A major problem is that the available tracer observations in high latitudes are clearly insufficient to permit a reasonably accurate calibration or validation of ocean models.

The oceanic CO_2 uptake of anthropogenic CO_2 is not very different from that of the one-dimensional box-diffusion model. The air-to-sea flux per unit area is about 50% higher in high latitudes than in low latitudes, because the perturbation is transported more rapidly to the deep sea. The sum of calculated oceanic CO_2 uptake plus observed atmospheric increase is smaller than the estimated emissions due to fossil fuel combustion and deforestation, a problem that is found by virtually all realistically designed carbon cycle models (IPCC, 1990). An interesting finding is that the response to an atmospheric CO_2 pulse of the HILDA model with a depth-dependent eddy diffusivity is quite similar to that of the 3-dimensional General Ocean Circulation Model discussed by Sarmiento et al. (1992).

9. Acknowledgments

REFERENCES

Bacastow, R. 1981. Numerical evaluation of the evasion factor. In: *Carbon Cycle Modelling* (ed. B. Bolin). SCOPE 16. Wiley, 95–101.

Broecker, W. S., Peng, T.-H. and Eng, R. 1980. Modeling the carbon system. *Radiocarbon 22*, 565–580.

Broecker, W. S. and Peng, T.-H. 1982. *Tracers in the sea*. Eldigio Press, Lamont-Doherty Geological Observatory, Palisades, N.Y.

Broecker, W. S., Peng, T.-H., Östlund, G. and Stuiver, M. 1985. The distribution of bomb radiocarbon in the ocean. *J. Geophys. Res. 90*, 6953–6970.

Druffel, E. M. and Suess, H. E. 1983. On the radiocarbon record in banded corals. *J. Geophys. Res. 88*, 1271–1280.

Druffel, E. M. and Benavides, L. M. 1986. Input of excess CO_2 to the surface ocean based on $^{13}C/^{12}C$ ratios in a banded Jamaica sclerosponge. *Nature 321*, 58–61.

Enting, I. G. and Pearman, G. I. 1987. Description of a one-dimensional carbon cycle model calibrated using techniques of constrained inversion. *Tellus 39B*, 459–476.

Friedli, H., Loetscher, H., Oeschger, H., Siegenthaler, U. and Stauffer, B. 1986. Ice core record of the $^{13}C/^{12}C$ ratio of atmospheric carbon dioxide in the past two centuries. *Nature 324*, 237–238.

Gargett, A. E. 1976. An investigation of the occurrence of oceanic turbulence with respect to finestructure. *J. Phys. Oceanogr. 6*, 139–156.

Gargett, A. E. 1984. Vertical diffusivity in the ocean interior. *J. Marine Res. 42*, 359–393.

Garrett, C. 1979. Mixing in the ocean interior. *Dyn. Atmos. Oceans 3*, 239–265.

Hoffert, M. I. 1989. The ocean in one dimension: upwelling, turbulence, temperature, oxygen, nutrients and carbon. *3rd Internat. Conference on Analysis and evaluation of atmospheric CO_2 data*, extended abstracts. Report E.P.M.R.P. No. 59, pp. 195–201. WMO, Geneva.

Intergovernmental Panel on Climate Change (IPCC), 1990. *Climate change, the IPCC scientific assessment*. WMO/UNEP. Cambridge University Press.

Joos, F., Sarmiento, J. L. and Siegenthaler, U. 1991a. Estimates of the effect of Southern Ocean iron fertilization on atmospheric CO_2 concentrations. *Nature 349*, 772–775.

Joos, F., Siegenthaler, U. and Sarmiento, J. L. 1991b. Possible effects of iron fertilization in the Southern Ocean on atmospheric CO_2 concentration. *Global Biogeochem. Cycles 5*, 135–150.

Junkins, J. L. 1978. *An introduction to optimal estimation of dynamical systems*. Sijthoff & Noordhoff, Alphen NL.

Keeling, C. D., Bacastow, R. B., Carter, A. F., Piper, S. C., Whorf, T. P., Heimann, M., Mook, W. G. and Roeloffzen, H. 1989a. A three dimensional model of atmospheric CO_2 transport based on observed winds: 1. Analysis of observational data. *Geophysical Monograph 55*, 165–236.

Keeling, C. D., Piper, S. C. and Heimann, M. 1989b. A three dimensional model of atmospheric CO_2 transport based on observed winds: 4. Mean annual gradients and interannual variations. *Geophysical Monograph 55*, 305–363.

Knox, F. and McElroy, M. B. 1984. Changes in atmospheric CO_2: influence of the marine biota at high latitudes. *J. Geophys. Res. 89*, 4629–4637.

Levitus, S. 1982. *Climatological atlas of the world oceans*. NOAA Professional Paper 13, US Govt. Printing Off., Washington, D.C., 133 pp.

Maier-Reimer, E. and Hasselmann, K. 1987. Transport and storage of CO_2 in the ocean, an inorganic ocean-circulation carbon cycle model. *Climate Dynamics 2*, 63–90.

Marland, G. 1989. Fossil fuels CO_2 emissions. *CDIAC Communications, Winter 1989*. Carbon Dioxide Information Analysis Center, Oak Ridge National Laboratory, Oak Ridge, TN. 1–3.

Mook, W. G. 1986. ^{13}C in atmospheric CO_2. *Netherlands J. Sea Research 20*, 211–223.

Neftel, A., Moor, E., Oeschger, H. and Stauffer, B. 1985. Evidence from polar ice cores for the increase in atmospheric CO_2 in the past two centuries. *Nature 315*, 45–47.

Newell, R. E. 1963. The general circulation of the atmosphere and its effects on the movement of tracer substances. *J. Geophys. Res. 68*, 3949–3962.

Nozaki, Y., Rye, D. M., Turekian, K. K. and Dodge, R. E. 1978. A 200 year record of carbon-13 and carbon-14 variations in a Bermuda coral. *Geophys. Res. Lett. 5*, carbon-13 and carbon-14 variations in a Bermuda coral. *Geophys. Res. Lett. 5*, 825–828.

Oeschger, H., Siegenthaler, U., Schotterer, U. and Gugelmann, A. 1975. A box diffusion model to study the carbon dioxide exchange in nature. *Tellus 27*, 168–192.

Peng, T.-H., Takahashi, T. and Broecker, W. S. 1987. Seasonal variability of carbon dioxide, nutrients and oxygen in the North Atlantic surface water: observations and a model. *Tellus 39B*, 439–458.

Pond, S. and Pickard, G. L. 1983. *Introductory dynamical oceanography*. Pergamon Press, Oxford.

Rotty, R. M. and Masters, C. D. 1985. Carbon dioxide from fossil fuel combustion. In: *Atmospheric carbon dioxide and the global carbon cycle* (ed. J. Trabalka). DOE/ER-0239, U.S. Dept. of Energy, Washington, DC, 20545, 63–80.

Sarmiento, J. L. 1983. A simulation of bomb tritium entry into the North Atlantic Ocean. *J. Phys. Oceanogr. 13*, 1924–1939.

Sarmiento, J. L., Feely, H. W., Moore, W. S., Bainbridge, A. E. and Broecker, W. S. 1976. The relationship between vertical eddy diffusion and buoyancy gradient in the deep sea. *Earth Planet. Sci. Letters 32*, 357–370.

Sarmiento, J. L. and Rooth, C. G. H. 1980. A comparison of vertical and isopycnal mixing models in the deep sea based on radon 222 measurements. *J. Geophys. Res. 85*, 1515–1518.

Sarmiento, J. L. and Toggweiler, J. R. 1984. A new model for the role of the oceans in determining atmospheric P_{CO_2}. *Nature 308*, 621–624.

Sarmiento, J. L., Orr, J. C. and Siegenthaler, U. 1992. A perturbation simulation of CO_2 uptake in an Ocean General Circulation Model. *J. Geophys. Res. 97*, 3621–3645.

Shaffer, G. and Sarmiento, J. L. 1992. Biogeochemical cycling in the global ocean 1: A new, analytical model with continuous vertical resolution and high latitude dynamics. *J. Geophys. Res.*, in press.

Siegenthaler, U. 1983. Uptake of excess CO_2 by an outcrop-diffusion model of the ocean. *J. Geophys. Res. 88*, 3599–3608.

Siegenthaler, U. 1986. Carbon dioxide: its natural cycle and anthropogenic perturbation. In: *The rôle of air-sea exchange in geochemical cycling* (ed. P. Buat-Ménard). Reidel, 209–247.

Siegenthaler, U. and Münnich, K. O. 1981. $^{13}C/^{12}C$ fractionation during CO_2 transfer from air to sea. In: *Carbon cycle modelling* (ed. B. Bolin). SCOPE 16. Wiley, 249–257.

Siegenthaler, U. and Wenk, T. 1984. Rapid atmospheric CO_2 variations and ocean circulation. *Nature 308*, 624–625.

Siegenthaler, U. and Oeschger, H. 1987. Biospheric CO_2 emissions during the past 200 years reconstructed by deconvolution of ice core data. *Tellus 39B*, 140–154.

Siegenthaler, U., Friedli, H., Loetscher, H., Moor, E., Neftel, A., Oeschger, H. and Stauffer, B. 1988. Stable-isotope ratios and concentration of CO_2 in air from polar ice cores. *Annals of glaciology 10*, 1–6.

Stuiver, M. and Pollach, H. 1977. Discussion reporting of ^{14}C data. *Radiocarbon 19*, 355–363.

Stuiver, M., Östlund, H. G. and McConnaughey, T. A. 1981. GEOSECS Atlantic and Pacific results. In: *Carbon Cycle Modelling* (ed. B. Bolin). SCOPE 16. Wiley, 201–222.

Stuiver, M. and Quay, P. 1981. Atmospheric ^{14}C changes resulting from fossail fuel CO_2 release and cosmic ray flux variability. *Earth Planet. Sci. Lett. 53*, 349–362.

Takahashi, T., Kaiteris, P., Broecker, W. S. and Bainbridge, A. E. 1976. An evaluation of the apparent dissociation constants of carbonic acid in seawater. *Earth Planet. Sci. Letters 32*, 458–467.

Tans, P. P. 1981. A compilation of bomb-^{14}C data for use in global carbon cycle models. In: *Carbon cycle modelling* (ed. B. Bolin). SCOPE 16. Wiley, 131–158.

Tans, P. P., Fung, I. Y. and Takahashi, T. 1990. Observational constraints on the global atmospheric CO_2 budget. *Science 247*, 1431–1438.

Toggweiler, J. R., Dixon, K. and Bryan, K. 1989a. Simulations of radiocarbon in a coarse resolution world ocean model 1. Steady state prebomb distributions. *J. Geophys. Res. 94*, 8217–8242.

Toggweiler, J. R., Dixon, K. and Bryan, K. 1989b. Simulations of radiocarbon in a coarse resolution world ocean model 2. Distributions of bomb-produced carbon-14. *J. Geophys. Res. 94*, 8243–8264.

Wanninkhof, R. 1992. Relationship between wind speed and gas exchange over the ocean. *J. Geophys. Res.*, in press.

Warner, M. J. 1988. Chlorofluoromethanes F-11 and F-12: Their solubilities in water and seawater and studies of their distributions in the South Atlantic and North Pacific Oceans. Ph. D. thesis, Univ. of California, San Diego.

Warner, M. J. and Weiss, R. F. 1985. Solubilities of chlorofluorocarbons 11 and 12 in water and seawater. *Deep-Sea Res. 17*, 721–735.

Weiss, R. F. 1974. Carbon dioxide in water and seawater: the solubility of a non-ideal gas. *Marine Chemistry 2*, 203–215.

Weiss, R. F., Bullister, J. L., Warner, M. J., Van Woy, F. A. and Salameh, P. K. 1990. *AJAX expedition chlorofluorocarbon measurements*. Scripps Institution of Oceanography Reference 90–6, La Jolla, Ca.

Welander, P. 1968. Theoretical forms for the vertical exchange coefficient in a stratified fluid. *Acta Soc. Sci. Litt. Gothoburgensis, Geophysica 1*. Gothenburg, Sweden.